Research Article

Latif Ahmad, Hafiz Ur Rahman, Umair Khan*, Nermeen Abdullah, and Samia Elattar

Insights into chemical reactions occurring in generalized nanomaterials due to spinning surface with melting constraints

https://doi.org/10.1515/phys-2025-0201
received March 19, 2025; accepted July 01, 2025

Abstract: The role of generalized nanoparticles was observed to be significant while increasing the surface area interaction between the base materials and the solid surface. The conductivity of such materials with the occurrence of similar and nonsimilar reactants has been observed to be very effective. Particularly, the processing of many rheological materials in industries is considered one of the significant applications. However, this study explored the unique features of the melting heat approach while considering the spinning motion of nanocomposite shear-thinning materials. The rheological material model was tested in the presence of autocatalytic reactions during its transparent conversion to a liquid state. Furthermore, the flow, temperature distribution, and nanoparticle concentration of the materials were represented by the conservation of momentum, concentration, and energy concepts. The leading problem is then presented using dimensionless local similar equations. The same equations are then numerically approximated by adopting one of the improved building three-stage formulas. The results were presented in terms of physical velocity, concentration, pressure, temperature, resistive forces, mass, and heat flow rates. The material dynamics are significantly reduced by plugging the higher relaxation time, and a reverse conduct is determined in the case of thermal analysis of the same materials. The melting heating factor and Brownian motion variation enhanced the flow speed and material temperature. On the other hand, a remarkable reduction in the material concentration was observed while uplifting similar and non-similar reaction factors. The method's accuracy is confirmed through a well-matched comparison with the literature.

Keywords: pseudo-plastic materials, dynamical reaction, rotating motion, collocation method.

Nomenclature

ρ (kg/m^3)	density fluid [M L^{-3}]
Ω (rad/s)	angular velocity [L^1 T^{-1}]
μ (kg/ms)	viscosity of the fluid [M^1 L^{-1} T^{-1}]
k (W/m K)	thermal conductivity
N_t	thermophoretic parameter
τ (N/m^2)	shear stress
η	dimensionless variable
N_b	Brownian motion parameter
Kc	HOM chemical reaction parameter
ρC_p (J/K)	specific heat capacity [M^0 L^2 T^{-2} K^{-1}]
u, v, w (m/s)	velocity components
m (J/kg)	melting heat parameter
∇	del operator
ν (m/s)	kinematic viscosity
D_B (m^2/s)	Brownian diffusivity coefficient
T (K)	temperature [K]
T_w (K)	wall temperature
C (mol/m^3)	concentration
A, B	species
C_f	skin friction
θ	dimensionless temperature
φ	dimensionless concentration
P (N/m^2)	pressure
Γ	relaxation time constant
A_1 (m/s)^2	first Rivlin–Ericksen tensor
$\vec{b}$ (N/m^3)	body force
$\vec{V}$ (m/s)	vector velocity
Sh	Sherwood number
Pr	Prandtl number

*** Corresponding author: Umair Khan,** Department of Mathematics, Saveetha School of Engineering, Saveetha Institute of Medical and Technical Sciences, Saveetha University, Chennai 602105, Tamil Nadu, India; Department of Mathematics, Faculty of Science, Sakarya University, Serdivan/Sakarya, 54050, Turkey,
e-mail: umairkhan@sakarya.edu.tr
Latif Ahmad, Hafiz Ur Rahman: Department of Mathematics, Shaheed Benazir Bhutto University, Sheringal Dir Upper, 18000, Pakistan
Nermeen Abdullah, Samia Elattar: Department of Industrial and Systems Engineering, College of Engineering, Princess Nourah bint Abdulrahman University, P.O. Box 84428, Riyadh 11671, Saudi Arabia

Sc	Schmidt number
Re	Reynold number
Nu	Nusselt number
I	identity tensor
Ks	HET chemical reaction
T_∞ (K)	ambient temperature
C_w (mol/m^3)	wall concentration
C_∞ (mol/m^3)	ambient concentration

1 Introduction

Non-Newtonian fluid flows gained massive attraction in the development of modern industries and different engineering technologies. In particular, the flow of non-Newtonian fluids has many applications such as polymer processing, slurry transport, and coating technologies. Wilkinson [1] presented the uses of such phenomena in terms of production, polymer extrusion of sheets, sheet emulsion, flow of plasma and blood, *etc.* Because of their rheological properties, the analysis of such fluids cannot be sufficiently described by modeling using the Navier–Stokes equations. However, the viscosity of non-Newtonian liquids depends on the shear stress and shear rate. These liquids exhibit a variety of complex flow behaviors and can be categorized into different types based on their responses to shear. Various non-Newtonian fluid models have been explored owing to their unique characteristics. Rashidi *et al.* [2] investigated the nonlinear nature of such materials. Yang *et al.* [3] illustrated the shear-thinning nature of the non-Newtonian flow of liquids across a porous material. Nazir *et al.* [4] deliberated the impact of chemical reactions on the flow of non-Newtonian liquids with heat and mass balance. Recently, Algehyne *et al.* [5] explored magnetic field effects on the transport of Maxwell liquid across a three-dimensional interface with passive boundaries.

The concept of nanofluids has become very attractive in recent advances in heat transmission and cooling processes with the inclusion of nanosized particles in the base liquids. However, nanofluids contain nanosized particles. As a result, with the inclusion of such particles, an increase in the thermal conductivity was noted, with the main purposes. Classically, nanomaterials used in nanoliquids contain metals, oxides, carbon nanotubes, and carbides. Choi and Eastman [6] were the first to introduce this phenomenon. They introduced nanoliquids, *i.e.*, fluids that contained nanosized particles (nanoparticles). Later, Buongiorno [7] established the generalized behavior of Brownian motion and thermophoretic forces for producing a unit temperature difference while introducing the motion of nonlinear materials. Kherbeet *et al.* [8] experimentally investigated the flow characteristics and heat transfer of nanofluids over microscale bidirectional step geometries. Hassan *et al.* [9] assessed the thermal impact of nanofluids when the base fluid viscosity was considered to be high. They addressed the concepts of Brownian and thermophoretic effects with a declining volume fraction. Payam *et al.* [10] explored the steady-state nanofluid motion through two parallel planes. Yasmin [11] conducted an analytical study of convective behavior featuring nonlinear properties in a nanolayered liquid film over a graded deforming interface [12]. A numerical analysis of magnetohydrodynamic water-based AA7072 nanofluid flow over a permeable stretching surface with slip conditions. Gangadhar *et al.* [13] investigated the simulation of radiative nonlinear heat dynamism on Buongiorno-modeled nanoliquids using porous inclined plates with adjustable chemical responses.

A homogenous (HOM) model refers to a system or model in which all the components or elements are identical or similar or consist of uniform entities that have the same characteristics and behavior, or a chemical reaction in which the reactants and products are in the same phase. HOM models are often used in various fields such as Physics, Chemistry, and Computer Science. Chaudhary and Merkin [14] were the first to introduce the phenomena of HOM and HET chemical reactions in the strongest boundary layer flow of the stagnation point. Rajesh *et al.* [15] studied the effects of HOM/HET reactions on oscillating magnetic boundary layer flow through a curved surface. Suleman *et al.* [16] analyzed the computational simulation of HOM/HET reactions and Newtonian heat transfer in silver–water nanofluid flowing past a nonlinearly stretched cylinder. A heterogeneous (HET) model refers to a system or model in which the components and elements are different or diverse, or a chemical reaction in which the reactants and products are in different phases. HET models are often used to study complex systems or situations in which the entities involved have different roles, capabilities, or characteristics. Hayat *et al.* [17] explored the Darcy–Forchheimer motion of carbon nanotube suspensions generated by a rotating disk subjected to convective heating, incorporating uniform and non-uniform chemical reactions. Doh *et al.* [18] analyzed how uniform and non-uniform reactions influence the nanofluid behavior induced by a rotating disk with varying thicknesses by applying the homotopy analysis technique.

The idea of melting heat is also called the heat of fusion, *i.e.*, the amount of heat energy needed to convert an element from its solid state to its liquid state at a fixed temperature and pressure. This is a particular type of energy phase transition. In fluid dynamics, the concept of melting heat is not directly applicable since fluids (liquids

and gases) do not possess a solid state with a well-defined melting point. Instead, they undergo phase transitions such as vaporization and condensation, which involve different thermodynamic properties like the heat of vaporization or heat of condensation. Roberts [19] was the first to initiate the melting concept by considering a hot air stream with the inclusion of an ice slab. Furthermore, Tien and Yen [20] examined the heat balance forced convective concept and observed the effect of melting between the surrounding fluid and the melting body. Yacob *et al.* [21] approximated the characteristics of the melting phenomenon during the approximation of velocity, temperature, and other related forces opposing the flow of liquid. Sadique *et al.* [22] explored the behavior of a thermally layered Powell–Eyring fluid, including the melting heat phenomenon. An analytical series solution was obtained using the homotopy analysis procedure. Shuguang *et al.* [23] and Mamatha *et al.* [24] employed this method owing to its accuracy and quick convergence.

A rotating disk in a fluid refers to a condition in which a solid disk is placed in a liquid medium and set to introduce rotational motion. This scenario has many applications and can be found in fields such as fluid dynamics, engineering, and physics, particularly in spin coating in thin film manufacturing, biomedical applications, and biomechanics. Karman and Uber [25] analyzed the incompressible viscous flow over an endless flat disk spinning at a constant angular speed. They pioneered the introduction of the concept of disk rotation in the presence of a viscous liquid with a constant density. Theoretical and experimental examinations of fluid motion due to disk rotation were first performed by Stewartson [26]. Watson and Wang [27] studied the unsteady flow over a rotating disk. Turkyilmazoglu [28] investigated the boundary layer development caused by a spinning disk using multiple generalized Newtonian fluid frameworks. Kelson and Desseaux [29] and Bachok *et al.* [30] explored nanofluid motion and heat transfer across a rotating porous disk. Recently, Ali *et al.* [31] made effective contributions in this direction. Aldhafeeri and Yasmin [32] conducted a computational study of hybrid nanofluid rotational flow over a unidirectionally stretching surface under velocity and thermal slip effects. Jawarneh *et al.* [33] explored the use of neural networks to examine magnetohydrodynamic nanofluid flow over a spinning disk, considering the effects of heat production and absorption.

1.1 Research gap and novelty statement

This study is the first to explore the rotational movement of shear-thinning materials using a higher-viscosity region approach. However, the entire study was further extended in the presence of chemical reactions, *i.e.*, HET and HOM chemical reactions. The same shear-thinning materials were further investigated with the additional inclusion of generalized nanomaterials. The melting heating concept was then used to illustrate the thermal analysis of complex materials. Additionally, for increasing the thermal conductivity, the Brownian motion and thermophoretic parameters are incorporated during this particular motion of the liquid. The influence of Brownian motion thickens the thermal boundary layer and elevates the temperature profiles, whereas the increase in thermophoresis significantly shifts the nanoparticle distribution and enhances the mass transfer rates during rotational flow. The newly rotating flow modeled problem will be considered for the numerical solution by implementing one of the collocation methods using the MATLAB software.

1.2 Limitations of the new work

The main limitations of this study are as follows.

- The flow features, heat, and mass balances are physically visualized in the form of graphs for low Reynolds numbers.
- The entire study is restricted to the assumptions used for the formulation of the newly stated problem.
- The modified collocation method cannot address the problem of singular points at the endpoints.
- The entire method is restricted to approximating the results in a very small domain.

1.3 Objectives of this work

The objectives of this work are as follows:

- To model the rotational flow of Williamson's fluid over a rotating disk in a generalized sense.
- To address the impacts of Brownian motion and thermophoretic parameters during the heat flow analysis.
- To analyze the influence of the HOM/HET chemical reaction during the mass flow analysis.
- To determine the approximate pressure, velocity, temperature, and concentration.

2 Problem description and mathematical model

Consider the three-dimensional, steady, symmetric, and incompressible motion of a Williamson fluid around a spinning cylindrical disk, accounting for both heat and mass transport. The disk rotates clockwise along the

z-axis with an angular velocity Ω. T_w and C_w are the surface temperature and concentration, respectively, and T_∞ and C_∞ are the ambient temperature and concentration, respectively, of the fluid (Figure 1).

The governing flow equations for this problem, namely continuity and momentum equations, are [34]

$$\nabla\cdot\mathbf{V} = 0, \tag{1}$$

$$\rho(\mathbf{V}\cdot\nabla\mathbf{V}) = -\nabla\cdot p + \nabla\cdot\tau, \tag{2}$$

where (u, v, w) are the components of the velocity field $\mathbf{V}$, P is the pressure, ρ is the density of the material, and τ is the stress tensor, which is defined as [34]:

$$\tau = \mu\mathbf{A_1}, \tag{3}$$

$$\mathbf{A_1} = (\nabla\boldsymbol{V}) + (\nabla\boldsymbol{V})^t. \tag{4}$$

By plugging Eqs. (3) and (4) in Eqs. (1) and (2), the leading equations in cylindrical coordinates are as follows [35,36]:

$$\frac{\partial u}{\partial r} + \frac{u}{r} + \frac{\partial w}{\partial z} = 0, \tag{5}$$

$$\rho\left(u\frac{\partial u}{\partial r} - \frac{v^2}{r} + w\frac{\partial u}{\partial z}\right) = -\frac{\partial p}{\partial r} + \frac{1}{r}\frac{\partial}{\partial r}(r\tau_{rr}) + \frac{\partial}{\partial z}\tau_{zr} - \frac{\tau_{\theta\theta}}{r}, \tag{6}$$

$$\rho\left(u\frac{\partial v}{\partial r} + \frac{uv}{r} + w\frac{\partial v}{\partial z}\right) = \frac{1}{r^2}\frac{\partial}{\partial r}(r^2\tau_{r\theta}) + \frac{\partial}{\partial z}\tau_{z\theta} + \frac{\tau_{\theta r} - \tau_{r\theta}}{r}, \tag{7}$$

$$\rho\left(u\frac{\partial w}{\partial r} + w\frac{\partial w}{\partial z}\right) = -\frac{\partial p}{\partial z} + \frac{1}{r}\frac{\partial}{\partial r}(r\tau_{rz}) + \frac{\partial}{\partial z}\tau_{zz}. \tag{8}$$

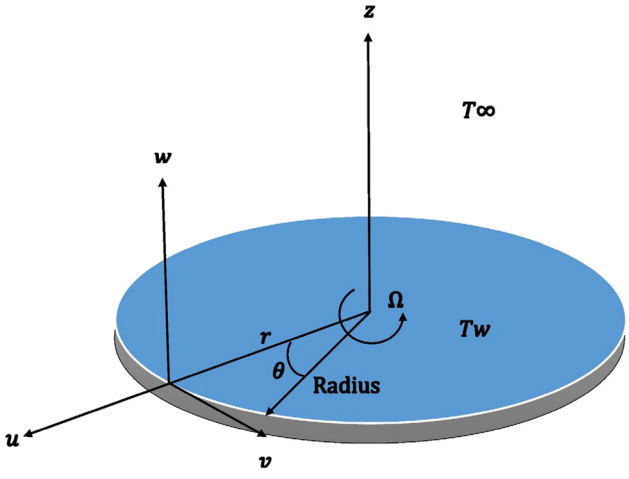

Figure 1: Schematic view of the proposed model.

The non-Newtonian Williamson fluid viscosity model (tensor) is $\mu = \mu_\circ\left[1 - (\Gamma^2\dot{\gamma})^{\frac{1}{2}}\right]^{-1}$, where Γ is the relaxation time constant and $\dot{\gamma}$ is given as follows [31]:

$$\dot{\gamma} = \left(2\left(\frac{\partial u}{\partial r}\right)^2 + 2\left(\frac{u}{r}\right)^2 + 2\left(\frac{\partial w}{\partial z}\right)^2 + \left(r\frac{\partial}{\partial r}\left(\frac{v}{r}\right)\right)^2 + \left(\frac{\partial v}{\partial z}\right)^2 + \left(\frac{\partial u}{\partial z} + \frac{\partial w}{\partial r}\right)^2\right)^{0.5}. \tag{9}$$

The boundary conditions (BCs) are

$$\begin{bmatrix}\text{At } z = 0, u = 0, v = r\Omega, w = 0,\\ \text{as } z \to \infty, u \to 0, v \to 0, w \to 0\end{bmatrix}. \tag{10}$$

Using $T = T(r, \theta, z)$ and $C = C(r, \theta, z)$ [34], the constitutive vector equations of the energy and concentration are as follows:

$$\rho C_\mathrm{p}\frac{\mathrm{d}T}{\mathrm{d}t} = -\nabla\cdot q + \nabla\left(D_\mathrm{B}\nabla C + \frac{D_T}{T_\infty}\nabla T\right), \tag{11}$$

$$\frac{\mathrm{d}C}{\mathrm{d}t} = -\nabla\cdot J + \nabla\left(D_\mathrm{B}\nabla C + \frac{D_T}{T_\infty}\nabla T\right) - K_c C_a C_b^2, \tag{12}$$

where q and J are the heat and mass fluxes, respectively, and are defined as

$$q = -k\nabla T, \tag{13}$$

$$J = -D\nabla C. \tag{14}$$

In the above expression, D refers to the diffusion coefficient, and the other term signifies the concentration gradient. Eqs. (11) and (12) are reduced as

$$\begin{bmatrix} u\frac{\partial T}{\partial r} + w\frac{\partial T}{\partial z} = \frac{k}{\rho c_\mathrm{p}}\left[\frac{\partial}{\partial r}\left(\frac{\partial T}{\partial r}\right) + \frac{1}{r}\frac{\partial T}{\partial r} + \frac{\partial}{\partial z}\left(\frac{\partial T}{\partial z}\right)\right]\\ +\tau\left[D_A\left(\frac{\partial C_b}{\partial r}\frac{\partial T}{\partial r} + \frac{\partial C_b}{\partial z}\frac{\partial T}{\partial z}\right) + \frac{\mathrm{DT}}{T_\infty}\left\{\left(\frac{\partial T}{\partial r}\right)^2 + \left(\frac{\partial T}{\partial z}\right)^2\right\}\right]\end{bmatrix}, \tag{15}$$

$$u\frac{\partial C_a}{\partial r} + w\frac{\partial C_a}{\partial z} = D_A\left(\frac{\partial^2 C_a}{\partial r^2} + \frac{1}{r}\frac{\partial C_a}{\partial r} + \frac{\partial^2 C_a}{\partial z^2}\right) - k_c C_a C_b^2, \tag{16}$$

$$u\frac{\partial C_b}{\partial r} + w\frac{\partial C_b}{\partial z} = D_B\left(\frac{\partial^2 C_b}{\partial r^2} + \frac{1}{r}\frac{\partial C_b}{\partial r} + \frac{\partial^2 C_b}{\partial z^2}\right) + \frac{D_T}{T_\infty}\left(\frac{\partial^2 T}{\partial z^2}\right) + k_s C_a C_b^2, \tag{17}$$

where D_A and D_T are the diffusion and thermophoretic coefficients, T_∞ is the ambient temperature, $k_c C_a C_b^2$ are the HOM reaction rate and $k_s C_a C_b^2$ the HET chemical reaction rate, (C_a, C_b) are the concentrations of the chemical reaction (A, B), respectively, and C_p is the specific heat.

The associated BCs are defined as:

$$\begin{bmatrix} T = T_w, C = C_w, \text{ at } z = 0 \\ T \to T_\infty, C \to C_a \text{ as } z \to \infty \end{bmatrix}. \tag{18}$$

All the aforementioned equations are dimensional, and by maintaining the physical significance, we converted the above set of equations into a dimensionless set of PDEs by introducing the following dimensionless similarity variables [37,38]:

$$\begin{bmatrix} \bar{r} = r/R, \bar{z} = z\mathrm{Re}^2/R, \bar{u} = u/\Omega R, \bar{v} = v/\Omega R, \\ \bar{w} = w\mathrm{Re}^{\frac{1}{2}}/\Omega R, \bar{p} = p\,\mathrm{Re}/\rho\Omega^2R^2, \\ \bar{\Gamma} = \Gamma\Omega\mathrm{Re}^{\frac{1}{2}}, \bar{\mu} = \mu/\mu_\circ, \bar{T} = (T - T_\infty)/(T_w - T_\infty), \\ \bar{C} = (C - C_\infty)/(C_w - C_\infty), \\ \bar{C}_a = C_a/C_\infty, \bar{C}_b = C_b/C_\infty. \end{bmatrix}. \tag{19}$$

Using the above transformations in Eqs. (5)–(9) and Eqs. (15)–(18), then we obtain

$$\frac{\partial \bar{u}}{\partial \bar{r}} + \frac{\bar{u}}{\bar{r}} + \frac{\partial \bar{w}}{\partial \bar{z}} = 0, \tag{20}$$

$$\bar{u}\frac{\partial \bar{u}}{\partial \bar{r}} - \frac{\bar{v}^2}{\bar{r}} + \bar{w}\frac{\partial \bar{u}}{\partial \bar{z}} = \frac{\partial}{\partial \bar{r}}\left(\bar{\mu}\frac{\partial \bar{u}}{\partial \bar{z}}\right), \tag{21}$$

$$\bar{u}\frac{\partial \bar{v}}{\partial \bar{r}} + \frac{\bar{u}\bar{v}}{\bar{r}} + \bar{w}\frac{\partial \bar{u}}{\partial \bar{z}} = \frac{\partial}{\partial \bar{z}}\left(\bar{\mu}\frac{\partial \bar{v}}{\partial \bar{z}}\right), \tag{22}$$

$$\bar{u}\frac{\partial \bar{w}}{\partial \bar{r}} = -\left(\bar{w}\frac{\partial \bar{w}}{\partial \bar{z}} + \frac{\partial \bar{p}}{\partial \bar{z}}\right) + \frac{1}{\bar{r}}\frac{\partial}{\partial \bar{r}}\left(\bar{\mu}\bar{r}\left(\frac{\partial \bar{u}}{\partial \bar{z}}\right)\right) + 2\frac{\partial}{\partial \bar{z}}\left(\bar{\mu}\frac{\partial \bar{w}}{\partial \bar{z}}\right), \tag{23}$$

$$\bar{u}\frac{\partial \bar{T}}{\partial \bar{r}} + \bar{w}\frac{\partial \bar{T}}{\partial \bar{z}} = \frac{1}{\mathrm{pr}}\left(\frac{\partial^2 \bar{T}}{\partial \bar{z}^2}\right) + N_b\left(\frac{\partial \bar{C}_b}{\partial \bar{z}} \cdot \frac{\partial \bar{T}}{\partial \bar{z}}\right) + N_t\left(\frac{\partial \bar{T}}{\partial \bar{z}}\right)^2, \tag{24}$$

$$\bar{u}\frac{\partial \bar{C}_a}{\partial \bar{r}} + \bar{w}\frac{\partial \bar{C}_a}{\partial \bar{z}} = \frac{1}{\mathrm{Sc}}\left(\frac{\partial^2 \bar{C}_a}{\partial \bar{z}^2}\right) - K_c\bar{C}_a\bar{C}_b = 0, \tag{25}$$

$$\bar{u}\frac{\partial \bar{C}_b}{\partial \bar{r}} + \bar{w}\frac{\partial \bar{C}_b}{\partial \bar{z}} = \frac{1}{\mathrm{Sc}}\left(\frac{\partial^2 \bar{C}_b}{\partial \bar{z}^2} + \frac{N_b}{N_t}\frac{\partial^2 \bar{T}}{\partial \bar{z}^2}\right) + k_sC_aC_b^2, \tag{26}$$

where

$$\dot{\bar{\gamma}} = \left[\left(\frac{\partial \bar{u}}{\partial \bar{z}}\right)^2 + \left(\frac{\partial \bar{v}}{\partial \bar{z}}\right)^2\right]^{\frac{1}{2}}. \tag{27}$$

The dimensionless factors appearing in the above equations are listed in the following table:

Schmidt number, Sc	$\frac{\nu}{D_B}$
Thermophoretic parameter, N_t	$\tau\frac{D_T(T_w - T_\infty)}{T_\infty\nu}$
Brownian motion parameter, N_b	$\tau\frac{D_BC_\infty}{\nu}$
Reynolds number, Re	$\frac{\Omega R^2}{\nu}$
Prandtl number, Pr	$\frac{\rho C_p\nu}{k}$
HOM reaction parameter, K_c	$\frac{k_cC_\infty^2}{\Omega}$
HET reaction parameter, K_s	$\frac{k_s\sqrt{\nu}}{D_A\sqrt{\Omega}}$

The BCs are reduced as

$$\begin{bmatrix} \text{at } z = 0 : u = 0, v = r\Omega, w = 0, T = T_w, C = C_w, \\ \text{as } z \to \infty : u = 0, v = 0, w = 0, T = T_w, C = C_\infty \end{bmatrix}. \tag{28}$$

For a smooth and accurate, less time-consuming solution, we need to transform the final PDEs to ODEs for which the following local similar variables are expressed as [37]

$$\begin{bmatrix} \eta = \bar{z}, \bar{u} = \bar{r}F(\eta), \bar{v} = \bar{r}G(\eta), \bar{w} = \bar{r}H(\eta), \\ \bar{T} = \theta(\eta), \bar{C}_a = \phi(\eta) \text{ and } \bar{C}_b = \varphi(\eta) \end{bmatrix}. \tag{29}$$

Then the final governing ODEs are obtained as

$$F^2 - G^2 + HF' - AF'' - ABF'^2F'' - ABF'G'G'' = 0, \tag{30}$$

$$2FG + HG' - AG'' - ABG'F'F'' - ABG'^2G'' = 0, \tag{31}$$

$$\begin{bmatrix} HH' + Q' - 2AF' - AB[F'^2G'^2] - 2AH'' \\ + 2ABH'[F'F'' + G'G''] = 0 \end{bmatrix}, \tag{32}$$

where

$$\left[A = \left\{1 - (\bar{\Gamma}^2(F^{'^2} + G^{'^2}))^{\frac{1}{2}}\right\}^{-1}\right]$$

and

$$\left[B = \bar{\Gamma}^2\left[1 - (\bar{\Gamma}^2(F'^2 + G'^2))^{\frac{1}{2}}\right]^{-1}[\bar{\Gamma}^2(F'^2 + G'^2)]^{-\frac{1}{2}}\right],$$

$$\theta'' = \mathrm{Pr}H\theta' - \mathrm{Pr}N_b(1 - \phi')\theta' - \mathrm{Pr}N_t\theta^{'^2}, \tag{33}$$

$$\varphi''(\eta) = \mathrm{Sc}H(\eta)\varphi'(\eta) + \mathrm{Sc}K_c\varphi'(\eta)(\phi(\eta))^2, \tag{34}$$

$$\phi''(\eta) = \mathrm{Sc}H(\eta)\varphi'(\eta) - \mathrm{Sc}\frac{N_b}{N_t}\theta''(\eta) - \mathrm{Sc}K_s\varphi(\eta)\phi(\eta). \tag{35}$$

If $\phi(\eta) + \varphi(\eta) = 1$, then for $\delta = 1$, Eqs. (34) and (35) are reduced to the following form:

$$\begin{aligned} \phi''(\eta) = {} & \mathrm{Sc}H\phi'(\eta) - \mathrm{Sc}\frac{N_b}{N_t}\theta''(\eta) \\ & + \mathrm{Sc}K_c\phi'(\eta)[1 - \phi(\eta)]^2. \end{aligned} \tag{36}$$

The system is subjected to the following BCs:

$$\begin{bmatrix} \mathrm{Pr}F + m\theta' = 0, G = 1, H = 0, \theta = 1, \phi - \mathrm{Ks}\phi' \text{ at } \eta = 0 \\ F = 0, G = 0, \theta = 0, \phi = 0 \text{ as } \eta \to \infty. \end{bmatrix}. \tag{37}$$

2.1 Engineering physical quantities

The physical quantities of interest are the skin friction coefficient (C_f), Nusselt number (Nu), and Sherwood number (Sh), which are presented as follows [38,39]:

$$C_f = \frac{\tau_w}{\rho r^2 \Omega^2}, \text{Nu} = \frac{-rk}{T_w - T_\infty}\frac{\partial T}{\partial z}, \text{Sh} = \frac{-r}{C_w - C_\infty}\frac{\partial C}{\partial z}. \quad (38)$$

By utilizing the above transformations to reduce Eq. (4) into ODEs, we have

$$\text{Re}^{0.5}\cdot\bar{r}C_{fr} = [1 - (\Gamma^2\cdot(F'^2 + G'^2))^{0.5}]^{-1}F', \quad (39)$$

$$\text{Re}^{0.5}\cdot\bar{r}C_{f\theta} = [1 - (\Gamma^2\cdot(F'^2 + G'^2))^{0.5}]^{-1}G', \quad (40)$$

$$\text{Re}^{0.5}\cdot\bar{r}\text{Nu} = -\theta'(0), \quad (41)$$

$$\text{Re}^{0.5}\cdot\bar{r}\text{Sh} = -\phi'(0). \quad (42)$$

2.2 Validation of the method

Table 1 presents the validation results of the proposed method. The outcomes were approximated using an improved collocation method in MATLAB. However, the results are compared with the works of Turkyilmazoglu [28], Kelson and Desseaux [29], and Bachok *et al.* [30], where it is observed that the method matches accurately by approximating the results in limiting cases.

2.3 Numerical method

The newly proposed problem is stated *via* Eqs. (44)–(49), and the BCs (50) are considered for an appropriate analysis *via* one of the modified collocation schemes. This method requires the input of the problem in terms of first-order ODEs and their corresponding BCs. After providing a weak initial guess, the method modifies the suggested guess for the next strong solution while using a default step size of 12 s with CPU time. The next updated solution is based on the improved boundary layer thickness, and the default tolerance level is noted for the same mesh point. The basic steps for the conversion of the newly proposed problem are as follows:

$$\begin{bmatrix} x_1 = F, \quad x_2 = F', \quad x_3 = G, \quad x_4 = G', \quad x_5 = H, \\ x_6 = Q, \\ x_7 = \theta, \quad x_8 = \theta', \quad x_9 = \phi, x_{10} = \phi', \text{where } x_1' = x_2 \end{bmatrix}. \quad (43)$$

Using Eq. (43), Eqs. (30)–(33) and (35) are converted to a system of first-order ODEs as follows:

$$x_2' = \frac{x_1^2 - x_3^2 + x_5x_2 - ABx_2x_4x_4'}{A + ABx_2^2}, \quad (44)$$

$$x_4' = \frac{2x_1x_3 + x_4x_5 - ABx_2x_4x_2'}{A + ABx_4^2}, \quad (45)$$

$$x_5' = -2x_1, \quad (46)$$

$$x_6' = 2Ax_2 + ABx_2(x_2^2 + x_4^2) - 4Ax_1 - 4ABx_1(x_2x_2^2 + x_4x_4^2) - x_1x_5 \ , \quad (47)$$

$$x_8' = \text{Pr}[x_5x_8 - N_b(1 - x_9)x_8 - N_tx_8^2], \quad (48)$$

$$x_9' = \text{Sc}\left(x_5x_9 - \frac{N_b}{N_t} + \text{Kc}x_9(1 - x_9)^2\right). \quad (49)$$

Here, $A = \left[1 - \{\bar{\Gamma}^2(x_2^2 + x_4^2)\}^{\frac{1}{2}}\right]^{-1}$, $B = \bar{\Gamma}^2\left[1 - \{\bar{\Gamma}^2(x_2^2 + x_4^2)\}^{\frac{1}{2}}\right]^{-1}\{\bar{\Gamma}^2(x_2^2 + x_4^2)\}^{-\frac{1}{2}}$.

The BCs are

$$\begin{bmatrix} \text{Pr}x_1 + mx_8 = 0, \quad x_3 = 1, \quad x_5 = 0, \\ x_7 = 1, \quad x_9 - \text{Ks}x_9' \text{ at } \eta = 0 \\ x_1 = 0, \quad x_3 = 0, \quad x_7 = 0, \quad x_9 = 0 \text{ as } \eta \to \infty \end{bmatrix}. \quad (50)$$

3 Results and discussion

The velocity field (V), temperature (T), and concentration (C) profiles are examined here with respect to the following parameters: the relaxation time constant (Γ), Schmidt

Table 1: Comparison between the current study and earlier published research

Measurable properties	Bachok *et al.* [30]	Kelson and Desseaux [29]	Turkyilmazoglu [28]	Present
$F'(0)$	0.5192	0.510233	0.51023262	0.51023255422
$-G'(0)$	0.6159	0.615922	0.61592201	0.61592171480
$-H'(0)$	—	0.884474	0.88447411	0.88445531887
$-\theta'(0)$	0.9337	—	0.93387794	0.93382648162

number (Sc), Prandtl number (Pr), thermophoretic parameter (N_t), Brownian motion parameter (N_b), and HOM/HET chemical reaction parameters (Kc) and (Ks. The values of all the parameters are fixed for finding the approximate results, *i.e.*,

Γ = 0.1, Pr = 0.7, N_t = 0.3, N_b = 0.7, Kc = 0.1, Ks = 4.5, Sc = 1, and m = 0.5.

The effect of Γ on the velocity components $F(\eta)$, $G(\eta)$, and$H(\eta)$ and pressure $P(\eta)$ of the fluid is shown in Figure 2(a)–(d). When the values of Γ are increased, then the radial and tangential velocity components and the pressure of the fluid are increased and the axial velocity component of the fluid is reduced. Physically, the fluid takes longer to adjust to changes in flow conditions, leading to more pronounced radial and tangential velocities as the fluid redistributes its momentum and slows down the adjustment of the fluid along the axial direction, potentially leading to reduced axial velocity. Fluid takes longer to equilibrate, resulting in higher radial pressure gradients to achieve balance within the flow. The contribution of the melting heat parameter m to the radial velocity component of the fluid is presented in Figure 3, where the melting heat parameter m enhanced $F(\eta)$. Physically, the melting heat parameter can influence the radial velocity field in a fluid during motion by affecting the distribution of the temperature gradient, which can alter the viscosity and density of the fluid. This can lead to changes in fluid flow patterns, including variations in radial velocity profiles and the formation of different flow structures. The contribution of the Prandtl number to the radial velocity component and temperature of the fluid is shown in Figure 4(a) and (b). A higher Prandtl number reduced the radial velocity component and temperature of the fluid. The Prandtl number affects the boundary layer development and heat transfer characteristics of the fluid flow. In terms of the radial velocity component, a higher Prandtl number typically results in a more pronounced boundary layer and slower radial velocity near the walls, as thermal diffusion

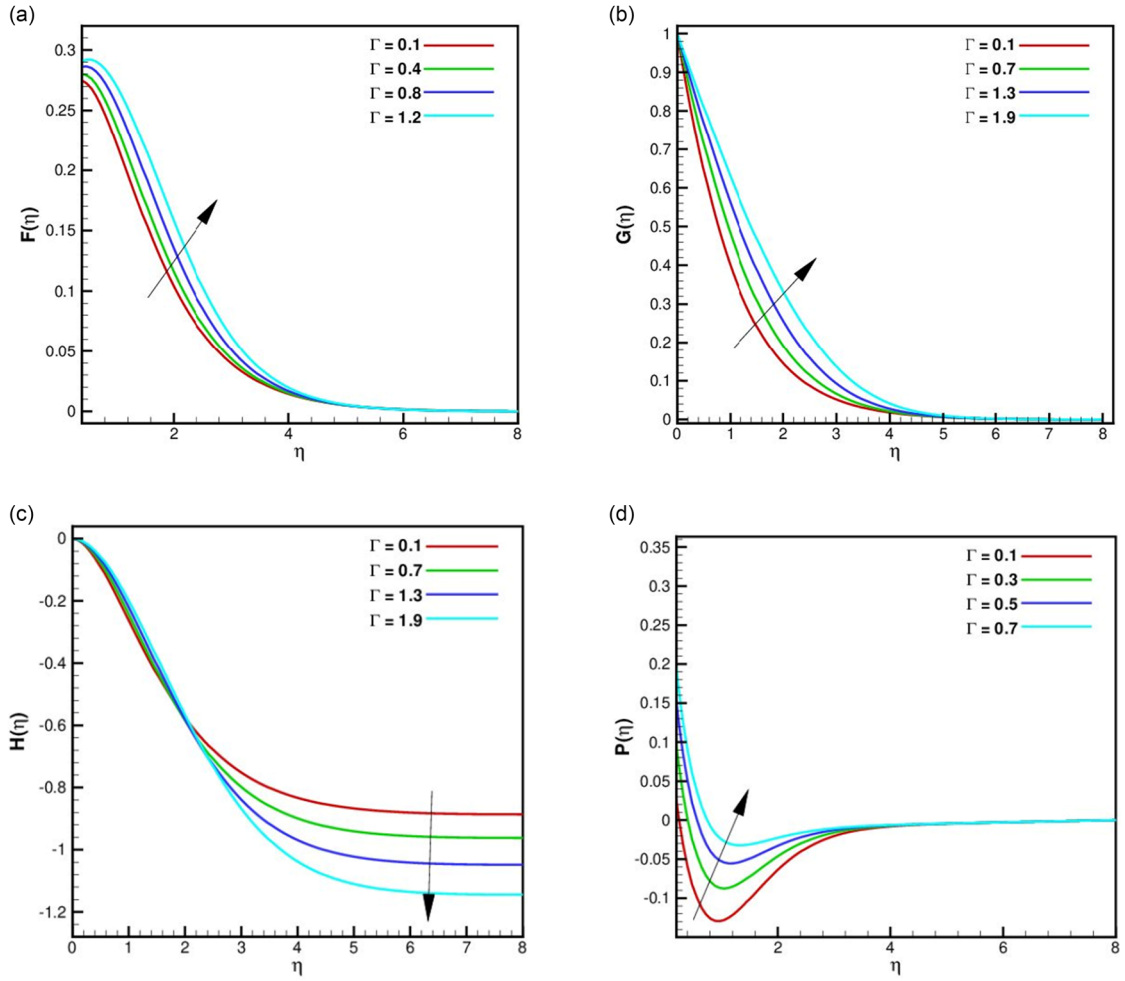

Figure 2: (a)–(d) Impact of Γ on the velocity components and pressure of the fluid.

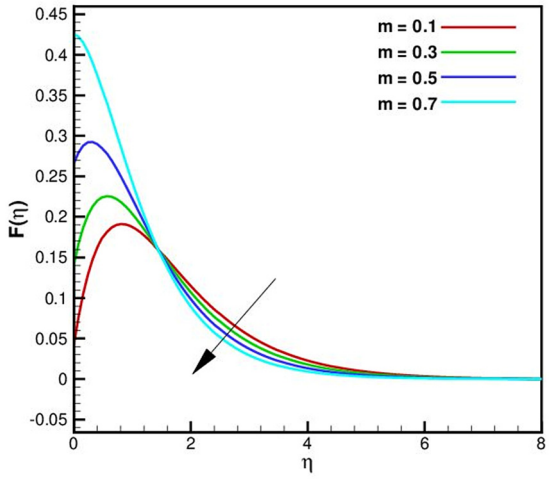

Figure 3: Influence of m on $F(\eta)$.

dominates over momentum diffusion. The Prandtl number influences the reduction in the thermal boundary layer thickness. In heat transfer scenarios, the Pr governs the comparative growth of the momentum and thermal boundary layers. When Pr increased, the thermal diffusivity of the fluid decreased, causing the thermal boundary layer to become thinner. The effects of (N_t) and (N_b) on the temperature and concentration fields of the fluid are shown in Figure 5(a)–(d). The thermophoretic parameter enhanced the temperature and concentration fields, whereas the Brownian motion parameter enhanced the temperature and reduced the concentration of the fluid. Physically, Brownian motion increases the kinetic energy of the particles in the fluid, leading to more collisions and thus more energy transfer between the particles. This increased energy transfer can increase the temperature. In the presence of temperature gradients, particles with different thermophoretic motilities experience forces that drive them toward regions of higher or lower temperatures, depending on their properties. (N_b) has a significant physical effect on the concentration field in the fluid. In simple terms, N_b influences the spread and movement of particles within the fluid, leading to changes in the concentration distribution over time. N_b impacts the stochastic movement of particles in the fluid. As the (N_b) factor enhanced, the particle exhibited more rapid and erratic movement, leading to greater dispersion throughout the fluid. The thermophoretic motion factor influences the concentration field in a fluid by affecting particle movement in response to temperature gradients. When a temperature gradient exists in a fluid, the thermophoretic motion parameter influences the migration of particles, leading to changes in the concentration distribution. Essentially, it affects the movement of particles in response to temperature differences, which in turn affects the concentration field within the fluid. The effects of the HOM/HET reaction parameter and Schmidt number on the concentration field are examined. For a higher HOM reaction parameter, the concentration of the fluid is reduced, and when the HET reaction parameter is varied, the concentration of the fluid is decreased. With an increase in the Schmidt number, the concentration field increased, as shown in Figure 6(a)–(c). It is clear that Kc and Ks decrease the concentration distribution because a large quantity of reactants is involved in the HOM reaction. Because Sc is the ratio of momentum diffusivity to mass diffusivity, higher Sc values indicate greater momentum diffusivity, resulting

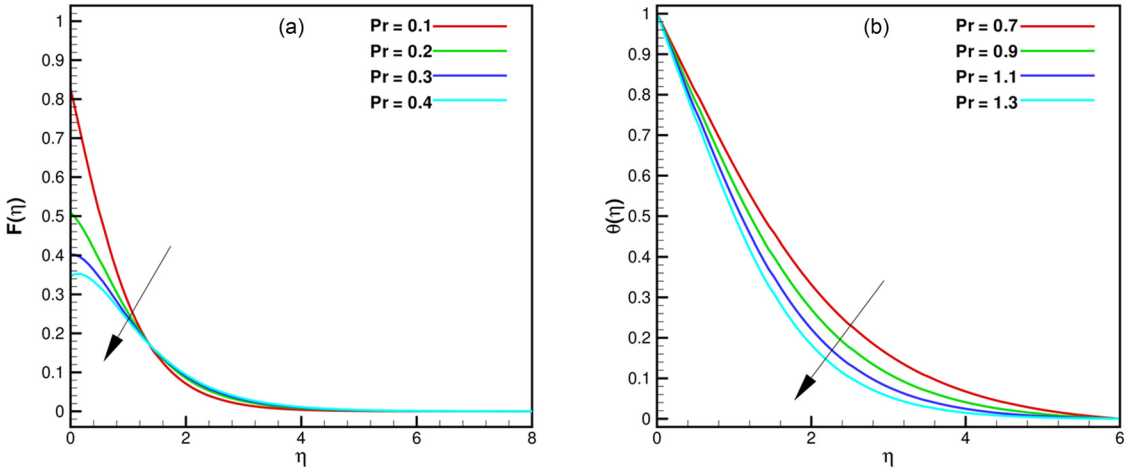

Figure 4: (a) and (b) Influence of Pr on $F(\eta)$ and $\theta(\eta)$.

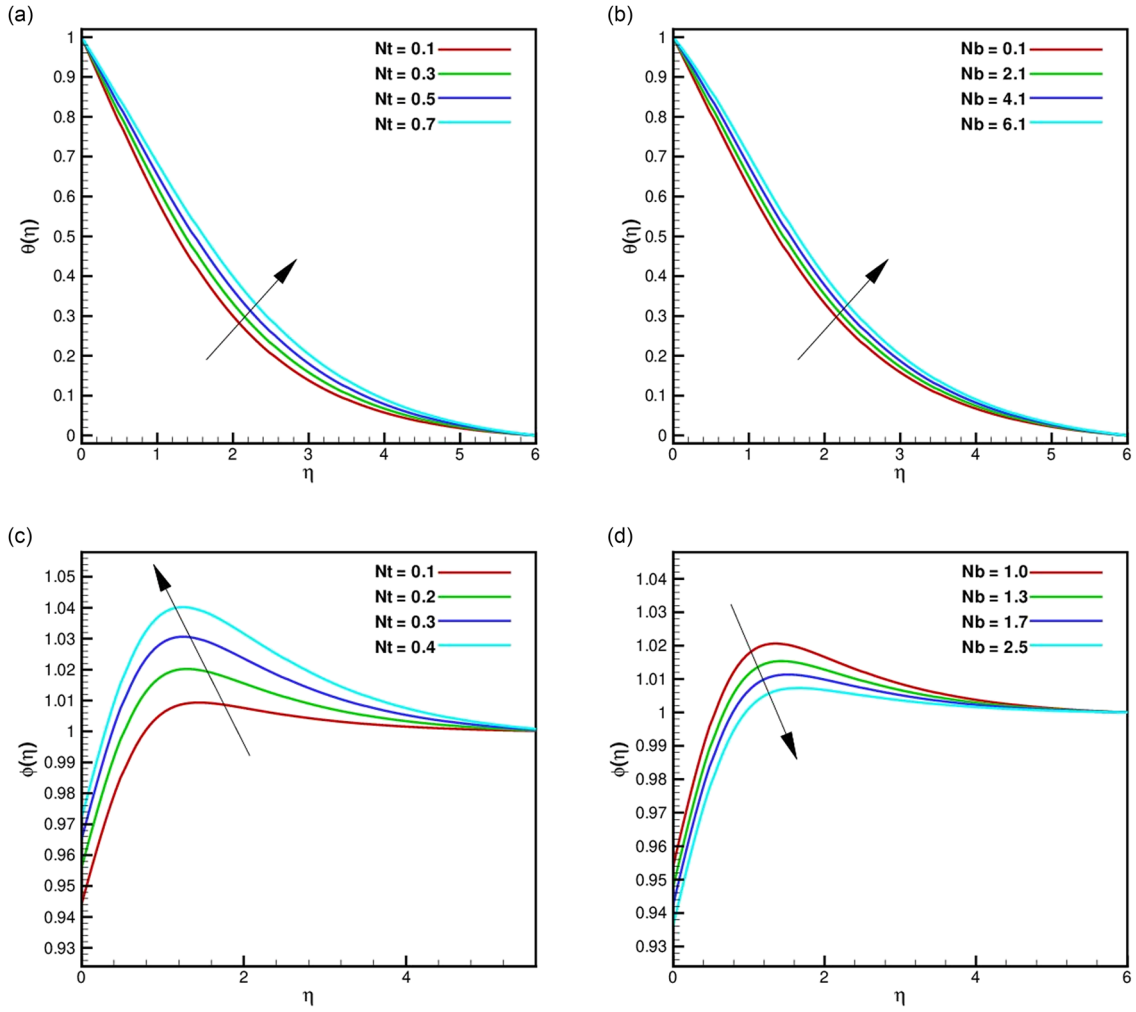

Figure 5: (a)–(d) Impact of Brownian and thermophoretic parameters on $\theta(\eta)$ and $\varphi(\eta)$ fields.

in an improved concentration profile. The contributions of the relaxation time constant Γ, melting heat parameter m, and the Prandtl number Pr to the radial and tangential skin frictions are shown in Table 2. The relaxation time constant enhanced the radial and tangential skin frictions. The variation in the Prandtl number tends to increase the radial and reduce the tangential skin friction, and a higher Prandtl number usually results in thicker boundary layers, leading to increased radial skin friction. The melting heat parameter typically reduces the radial and increases the tangential skin fraction because a higher melting heat parameter indicates that more heat is required to cause the fluid to transition from a solid to a liquid state. The effects of the thermophoretic, Brownian motion, and HOM/HET chemical reaction parameters on the Nusselt and Sherwood numbers are shown in Table 3. The thermophoretic parameter reduced the Nusselt and Sherwood numbers, and the Brownian motion parameter reduced the Nusselt number and enhanced the Sherwood number. The HOM reaction parameter enhanced and the HET reaction parameter reduced the Nusselt and Sherwood numbers. The thermophoretic parameter reduced the Nusselt and Sherwood numbers because it tends to drive particles away from hotter regions, hindering heat and mass transfer. Conversely, the Brownian motion parameter reduces the Nusselt number because it leads to more chaotic particle movement, making it harder for them to carry heat; however, it enhances the Sherwood number as it increases the chances of particles interacting with the fluid, improving mass transfer. HOM reactions enhance the Nusselt and Sherwood numbers because they increase the contact between the fluid and the reacting species, promoting heat and mass transfer. However, HET reactions reduce these numbers because they create surface barriers that impede the transfer of heat and mass between the fluid and the solid surface where the reaction occurs.

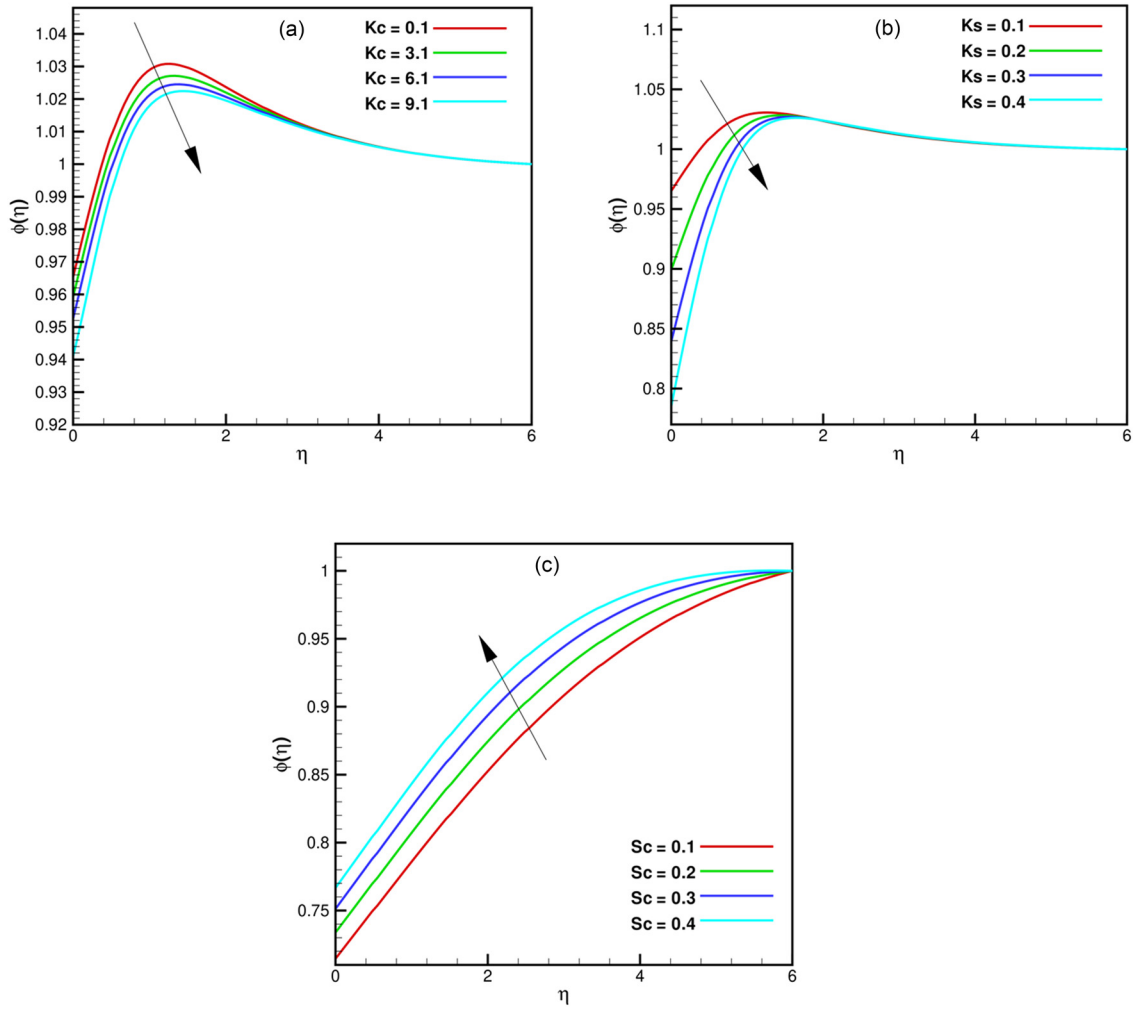

Figure 6: (a)–(c) Impact of HOM/HET reactions and Schmidt number on $\varphi(\eta)$.

Table 2: Impact of Γ, Pr, and the melting heat parameter on radial and tangential skin frictions

Parameters			$(\mathrm{Re}\cdot\bar{r}^2)^{\frac{1}{2}}C_{fr}$	$(\mathrm{Re}\cdot\bar{r}^2)^{\frac{1}{2}}C_{f\theta}$
Γ	Pr	M		
0.1	0.7	0.5	0.5284	0.6316
0.3			0.5674	0.6647
0.5			0.6079	0.6989
0.1	0.5	0.5	0.2442	0.8989
	0.7		0.2915	0.8596
	1.0		0.3310	0.8254
	0.7	0.1	0.4918	0.6708
		0.4	0.3518	0.8068
		0.7	0.1410	0.9792

Table 3: Impact of N_b, N_t, Kc, and Ks parameters on Nu and Sh

Parameters				$\mathrm{Re}^{\frac{1}{2}}\cdot\bar{r}\mathrm{Nu}$	$\mathrm{Re}^{\frac{1}{2}}\cdot\bar{r}\mathrm{Sh}$
N_b	N_t	Kc	Ks		
0.5	0.7	1.0	4.5	0.2205	−0.3685
0.6				0.2029	−0.3994
0.7				0.1877	−0.4265
	0.2			0.3252	−0.5613
	0.3			0.3119	−0.4420
	0.4			0.2994	−0.3791
		0.1		0.2607	−0.3196
		0.2		0.2611	−0.3171
		0.3		0.2615	−0.3145
			0.1	0.3532	−0.1003
			0.2	0.3278	−0.1559
			0.3	0.3127	−0.1877

4 Concluding remarks and future work

This study was initiated to explore the unique features of the rotary motion of a dilatant fluid, such as the Williamson material. The same materials were effectively analyzed in the presence of generalized Brownian motion and the melting heat concept. The thermal analysis of the materials was explicitly demonstrated by incorporating the influence of the thermophoretic forces. Two types of chemical reactions were tested to explore the significance of the material concentration. Each new impact was then presented through graphs of flow speed, concentration, energy, and pressure. The valid physical characteristics of the material were briefly demonstrated for specific values of the various controlling parameters. This typical work can be further extended by considering the clockwise and anti-clockwise rotations of the stretching/shrinking double disks. The key findings of this study are as follows:

- The melting heat parameter reduced the flow speed away from the disk surface.
- The material factor enhanced the $F(\eta)$ and $G(\eta)$ components of the flow speed.
- Both thermophoresis and Brownian motion increase the material temperature.
- The material concentration was enhanced for higher values of the thermophoretic force, and a reverse trend was observed for increasing values of N_b.
- Higher HET and HOM reaction factors reduced the material concentration.
- The resistive forces in the radial direction were reduced, and the opposite conduct was observed in the case of the tangential resistive force when considering a higher melting factor.

Acknowledgments: The authors extend their appreciation to the support of Princess Nourah bint Abdulrahman University Researchers Supporting Project number (PNURSP2025R730), Princess Nourah bint Abdulrahman University, Riyadh, Saudi Arabia.

Funding information: The support of Princess Nourah bint Abdulrahman University Researchers Supporting Project number (PNURSP2025R730), Princess Nourah bint Abdulrahman University, Riyadh, Saudi Arabia, is acknowledged.

Author contributions: All authors have accepted responsibility for the entire content of this manuscript and approved its submission.

Conflict of interest: The authors state no conflict of interest.

Data availability statement: All data generated or analyzed during this study are included in this published article.

References

[1] Wilkinson WL. The drainage of a Maxwell liquid down a vertical plate. Chem Eng J. 1970;1(3):255–7.
[2] Rashidi M, Bagheri MS, Momoniat E, Freidoonimehr N. Entropy analysis of convective MHD flow of third grade non-Newtonian fluid over a stretching sheet. Ain Shams Eng J. 2017;8(1):77–85.
[3] Yang X, Tang Y, Li M, Li C, Wang W, Li X, et al. Effect of shear-thinning of non-Newtonian fluid on the crossover from capillary fingering to viscous fingering in porous media. Phys Lett A. 2022;449:128364.
[4] Nazir S, Kashif M, Zeeshan A, Alsulami H, Ghamkhar M. A study of heat and mass transfer of Non-Newtonian fluid with surface chemical reaction. J Indian Chem Soc. 2022;99(5):100434.
[5] Algehyne EA, Lone SA, Raizah Z, Eldin SM, Saeed A, Galal AM. Mechanical characteristics of MHD of the non-Newtonian magnetohydrodynamic Maxwell fluid flow past a bi-directional convectively heated surface with mass flux conditions. Front Mater. 2023;10:11331–3.
[6] Choi SUS, Eastman JA. Enhancing thermal conductivity of fluids with nanoparticles. Int Mech Eng Congr Expo. 1995;231(66):99–105.
[7] Buongiorno J. Convective transport in nanofluids. J Heat Transf. 2006;18:240–50.
[8] Kherbeet AS, Mohammed HA, Salman BH, Ahmed HE, Alawi OA, Rashidi MM. Experimental study of nanofluid flow and heat transfer over microscale backward- and forward-facing steps. Exp Therm Fluid Sci. 2015;65:13–21.
[9] Hassan M, Mebarek-Oudina F, Faisal A, Ghafar A, Ismail AI. Thermal energy and mass transport of shear thinning fluid under effects of low to high shear rate viscosity. Int J Thermofluids. 2022;15:100176.
[10] Payam J, Narimisa H, Bahram J, Ganji DD. Micro-polar nanofluid in the presence of thermophoresis, hall currents, and Brownian motion in a rotating system. Mod Phys Lett. 2023;14:2250197.
[11] Yasmin H. Analytical investigation of convective phenomena with nonlinearity characteristics in nanostratified liquid film above an inclined extended sheet. Nanotechnol Rev. 2024;13(1):20240064.
[12] Aldhafeeri AA, Yasmin H. A numerical analysis of magnetohydrodynamic water-based AA7072 nanofluid flow over a permeable stretching surface with slip conditions. J Radiat Res Appl Sci. 2025;18(2):101356.
[13] Gangadhar K, Chandrika NG, Dinarvand S. Simulation of radiative nonlinear heat dynamism on Buongiorno-modeled nanoliquid through porous inclined plate with adjustable chemical response. Mod Phys Lett B. 2024;38(34):2450347.
[14] Chaudhary MA, Merkin JH. A simple isothermal model for HOM - HET reactions in boundary-layer flow. I Equal diffusivities. Fluid Dyn Res. 1995;16:311–33.
[15] Rajesh V, Beg AO, Sridevi C. Finite difference analysis of unsteady MHD free convective flow over moving semi-infinite vertical cylinder with chemical reaction and temperature oscillation effects. J Appl Fluid Mech. 2016;9:157–67.
[16] Suleman M, Ramzan M, Ahmad S, Lu D. Numerical simulation for homogeneous–heterogeneous reactions and Newtonian heating

in the silver-water nanofluid flow past a nonlinear stretched cylinder. Phys Scr. 2019;94(8):085702.
[17] Hayat T, Haider F, Muhammad T, Ahmad B. Darcy–Forchheimer flow of carbon nanotubes due to a convectively heated rotating disk with homogeneous–heterogeneous reactions. J Therm Anal Calorim. 2019;137:1939–49.
[18] Doh DH, Muthtamilselvan M, Swathene B, Ramya E. Homogeneous and heterogeneous reactions in a nanofluid flow due to a rotating disk of variable thickness using HAM. Math Comput Simul. 2020;168:90–110.
[19] Roberts L. On the melting of a semi-infinite body of ice placed in a hot stream of air. J Fluid Mech. 1958;4:505–28.
[20] Tien C, Yen YC. The effect of melting on forced convection heat transfer. J Appl Meteorol. 1965;4:523–7.
[21] Yacob NA, Ishak A, Pop I. Melting heat transfer in boundary layer stagnation-point flow towards a stretching/shrinking sheet in a micro polar fluid. Comput Fluids. 2011;47:16–21.
[22] Sadique R, Aisha A, Farooq M, Malik MY. Melting heat phenomenon in thermally stratified fluid reservoirs (Powell-Eyring fluid) with joule heating. Int Commun Heat Mass Transf. 2022;137:106196.
[23] Shuguang L, Farhan A, Zaib A, Loganathan K, Sayed ME, Khan M, I. Bioconvection effect in the Carreau nanofluid with Cattaneo-Christov heat flux using stagnation point flow in the entropy generation: Micromachines level study. Open Phys. 2023;21(1):20220228.
[24] Mamatha SU, Devi RLV, Ameer AN, Ali SN, Madhusudhan RB, Raju CSK, et al. Multi-linear regression of triple diffusive convectively heated boundary layer flow with suction and injection: Lie group transformations. Int J Mod Phys. 2023;37(1):2350007.
[25] Karman V, Uber T. Laminare and turbulente Reibung. Z Angew Math Mech. 1921;1:233–52.
[26] Stewartson K. On the flow between two rotating coaxial disks. Proc Camb Phil Soc. 1953;49:333–41.
[27] Watson LT, Wang CY. Deceleration of a rotating disk in a viscous fluid. Phys Fluids. 1979;22(12):2267–9.
[28] Turkyilmazoglu M. Nanofluid flow and heat transfer due to a rotating disk. Z Angew Math Mech. 2014;94:139.
[29] Kelson N, Desseaux A. Note on porous rotating disk flow. ANZIAM J. 2000;42:C837–55.
[30] Bachok N, Ishak A, Pop I. Flow and heat transfer over a rotating porous disk in a nanofluid. Phys B: Condens Matter. 2011;406(9):1767–72.
[31] Ali F, Zaib A, Loganathan K, Saeed A, Seangwattana T, Kumam P, et al. Scrutinization of second law analysis and viscous dissipation on Reiner-Rivlin Nanofluid with the effect of bioconvection over a rotating disk. Heliyon. 2023;9(13091):1767–72.
[32] Aldhafeeri AA, Yasmin H. A numerical analysis of the rotational flow of a hybrid nanofluid past a unidirectional extending surface with velocity and thermal slip conditions. RAMS. 2024;63(1):20240052.
[33] Jawarneh Y, Yasmin H, Jan WU, Akbar A, Al-Sawalha MM. A neural networks technique for analysis of MHD nano-fluid flow over a rotating disk with heat generation/absorption. AIMS Math. 2024;9(11):32272–98.
[34] Ahmad L, Islam S, Alqahtani AM, Sarfraz M. Swirling motion of temperature-dependent chemical reactions and Arrhenius activation energy in Cross fluid. Int Commun Heat Mass Transf. 2024;159:108082.
[35] Griffiths PT. Flow of a generalized Newtonian fluid due to a rotating disk. J Non-Newtonian Fluid Mech. 2015;221:9–17.
[36] Turkyilmazoglu M. Fluid flow and heat transfer over a rotating and vertically moving disk. Phys Fluids. 2018;30(6):063605.
[37] Ming C, Liu K, Han K, Si X. Heat transfer analysis of Carreau fluid over a rotating disk with generalized thermal conductivity. Comp Maths. 2023;144:141–9.
[38] Mishra SR, Shamshuddin MD, Beg OA, Kadir A. Adomain computation of radiative-convective bi-directional stretching flow of a magnetic non-Newtonian fluid in porous media with homogeneous–heterogeneous reactions. Int J Mod Phys B. 2020;34(18):2050165.
[39] Kumar KG, Gireesha BJ, Rudraswamy NG, Gorla R. Melting heat transfer of hyperbolic tangent fluid over a stretching sheet with fluid particle suspension and thermal radiation. Commun Numer Anal. 2017;2:125–40.